



Determination of Mohr–Coulomb failure envelope, mechanical properties and UPV of commercial cement-lime mortar

Amrit Ghimire · Sarkar Noor-E-Khuda  · Shah Neyamat Ullah · Thuraichamy Suntharavadivel

Received: 7 October 2021 / Accepted: 5 April 2022 / Published online: 16 April 2022
© The Author(s) 2022

Abstract Mortar in masonry structures can be subjected to both uniaxial and triaxial loading. Determining the mechanical properties and/or failure criteria of the commonly used mortar is necessary for the structural performance assessment of new and existing masonry buildings using non-destructive testing and/or finite element modelling methods. In this paper, the stress–strain behaviour of a commercially available cement-lime mortar is investigated under uniaxial and triaxial loading. The axial compressive strength, modulus of elasticity, Mohr–Coulomb failure envelopes of the mortar are determined over a range of conditions. Mortar specimens were prepared with a

water to cementitious material ratio (w/cm) of 0.6–0.7 and were tested at curing ages of 3, 7, 14, and 28 days, under confining pressures of 0, 100, 250, 500 and 750 kPa. Ultrasonic pulse velocity (UPV) of the specimens were measured before the destructive testing. The results indicate that the influence of curing age and confining pressure on the axial compressive strength of the mortar can be predicted using proposed linear correlations between (i) The confining pressure and the axial compressive strength and (ii) The UPV and the axial compressive strength. From the test results, the strength parameters of the Mohr–Coulomb failure criterion were also determined. It is observed that cohesion is more sensitive to changes in curing age and w/cm than the friction angle, which varied between 32 and 33 degrees.

A. Ghimire
School of Engineering and Built Environment, Deakin University, Waurm Ponds VIC3216, Australia
e-mail: ghimirea@deakin.edu.au

S. Noor-E-Khuda (✉)
School of Engineering and Technology, Central Queensland University, Melbourne VIC3000, Australia
e-mail: s.noorekhuda@cqu.edu.au

S. N. Ullah
School of Engineering and Technology, Central Queensland University, Gladstone, QLD4680, Australia
e-mail: s.ullah@cqu.edu.au

T. Suntharavadivel
School of Engineering and Technology, Central Queensland University, Rockhampton QLD4701, Australia
e-mail: t.suntharavadivel@cqu.edu.au

Keywords Mortar · Triaxial loading · Uniaxial loading · Mohr–Coulomb criteria · UPV · Stress–strain

1 Introduction

In masonry, mortar is used as a binder material to connect the units (bricks/blocks). There has been an observed increase in the demand for masonry over time due to its simple and economic construction technique, easy availability of the constituents (units and mortar), aesthetically pleasing appearance and advantageous mechanical properties (high strength,



thermal and fire resistance [1–3]). Masonry is a composite, requiring an in-depth assessment of its constituents for an accurate estimation of its behaviour under different loading conditions. McNary and Abrams [3] reported that under axial compression loading, the units in masonry experience uniaxial compressive stress along the direction of loading and biaxial tensile stress along the sides. Mortar, on the other hand, experiences a triaxial compressive stress state, which is caused by the resistance provided by the units to sidewise expansion [4]. It was indicated that the behaviour of mortar is more significant in determining the overall performance of the masonry structure than the behaviour of bricks [3]. Mortar, being of weaker nature and the weaker material in masonry, limits the overall strength of the masonry structure [3, 4]. The bond between mortar and brick has a considerable role in the mechanics of masonry [3]. It is therefore important to investigate the behaviour of mortar under uniaxial (unconfined) and triaxial loading conditions.

The mechanical properties of mortar are influenced by changes in its composition, i.e., the aggregate-cement ratio [5], type of aggregate [6], type of binder material (i.e., cement, lime) [7, 8], and water-cement ratio (w/c) [9], which has been extensively studied by researchers. This article recognises the contribution of researchers (including [5–17]) on improving the mechanical properties and durability of mortar and producing sustainable and environmentally friendly mortar. Most research so far has focused on the uniaxial strength and durability of various types of mortar, where the composition of mortar are modified using industrial by-products, chemical additives, recycled aggregates, and various types of fibres [5–12]. Such mortars are produced precisely in an idealistic laboratory environment, not available commercially and rarely gets used by builders. On the contrary, commercial cement-lime masonry mortars are produced on a mass scale and have been extensively used by the Australian masonry construction industry. The absence of key mechanical properties (compressive strength, tensile strength, and modulus of elasticity) and parameters of the Mohr–Coulomb failure criterion (cohesion and angle of internal friction) of these commercial mortars, forces structural designers to assume arbitrary values of these key modelling parameters while simulating the mortar joints in masonry structures using the available finite

element (FE) modelling methods [18–20], which reduces the accuracy of the structural performance prediction of the existing masonry structures. As such, there is a need to determine the mechanical properties (under both uniaxial and triaxial loading) and Mohr–Coulomb strength parameters of the commercial mortars. Although the triaxial stress states and corresponding strength for concrete has been well acknowledged [21–26], no such research has hitherto been reported for commercial mortars [3, 4, 13–16, 27, 28] that is widely used by builders.

In general, the failure behaviour of the mortar joints in masonry is defined using the Mohr–Coulomb failure criterion [13, 22–28], shown in Eq. 1, which comprises a linear relationship between the shear strength (τ), normal stress (σ), cohesion (c) and the angle of internal friction (φ).

$$\tau = c + \sigma \tan \varphi \quad (1)$$

In the literature, Khoo [4] has extensively studied the triaxial compressive behaviour of mortar with varying composition and water cement ratio (w/c). Toufigh et al. [22] investigated the mechanical behaviour of polymer concrete under uniaxial and triaxial loading with varying confining pressure. It was reported in [4, 22] that the increase in confining pressure increased the compressive strength as well as the size of the failure envelope. Khoo [4] also plotted the stress–strain curve for varying confining pressure levels, developed the Mohr’s circles, and determined the volumetric contraction due to cell pressure and the effect of cell pressure on the modulus of elasticity, Poisson’s ratio and cracking pattern of the tested specimens. McNary and Abrams [3] numerically modelled the triaxial compression behaviour of mortar and the biaxial tension–compression behaviour of brick. Assaad et al. [13] conducted triaxial testing on concrete-equivalent mortar specimens to examine the influence of formwork pressure of self-consolidating concrete and estimated the lateral pressure from the cohesion values. Chen et al. [25] tested concrete specimens at different temperatures and at curing ages of 3, 7, 14, and 28 days.

While the destructive test methods are well regarded by the scientific community for their accuracy, recent developments in non-destructive test (NDT) methods have provided means for reliable on-site measurements. The common NDT methods adopted by researchers include ultrasonic pulse



velocity (UPV), rebound hammer, acoustic emission, ground penetration radar and laser scanning [29–33]. The UPV method is commonly used in assessing the mechanical properties of concrete and other quasi-brittle materials [1, 11, 31–33]. As such, UPV assessment of the commercial mortar is also incorporated in the present study considering its potential for quick and inexpensive onsite measurements.

In this paper, the mechanical properties of mortar under uniaxial and triaxial compressive loading are investigated through an extensive experimental program. The mortar reported in this work is the commercially available and most commonly used M3 type cement-lime masonry mortar as specified in the Australian Standard AS3700-2018 [34]. The mortar specimens were prepared with high w/cm to replicate site conditions while the confining pressure in the triaxial testing was selected to suit the triaxial stress state in masonry. Mortar specimens of different ages were tested and their stress–strain relationship, Mohr–Coulomb failure envelope, density, UPV, dynamic modulus of elasticity, strength envelope, correlation between axial compressive strength and confining pressures, correlation between UPV and age of the specimen, and correlation between axial compressive strength and UPV are presented. The effect of varying w/cm on the uniaxial and triaxial stress state is also studied.

2 Experimental program

Details of the test specimens, test material and experimental details are discussed in this section. All the tests were performed at the Perth Engineering Laboratory of Central Queensland University.

2.1 Description of test specimens and preparation

A commonly used and commercially available general-purpose M3 type Australian cement-lime masonry mortar [34] with a mix ratio of cement:lime:sand of 1:1:6 was used in the experimental program. Cylindrical specimens of varying dimensions were used by most researchers for triaxial testing. Assaad et al. [13] used specimens of 38 mm diameter and 90 mm height in the triaxial testing. The diameter of specimens used by [22, 26] and [28] was 50, 150 and 50.4 mm, respectively. After reviewing the available

literature [13] and considering mortar as a finer material than concrete, specimens of 38 ± 0.08 mm diameter and 100 ± 0.51 mm height were used for the uniaxial and triaxial testing. The w/c is another key parameter that dictates the material properties, strength, and workability of mortar. The w/c of a mortar mix is targeted to achieve sufficient workability in the fresh state and maximum strength in the hardened state. In general, a w/c of 0.4–0.5 is considered ideal for reaching the optimum strength and workability. The w/c used by researchers [13, 22] and [14] were 0.42, 0.36–0.5 and 0.5, respectively. Maintaining an exact w/c in a site condition can be challenging, where water is added to the dry mortar mix using approximation without accurately measuring the exact quantity. To ease the placement of mortar, the use of a higher w/c is advocated by [35]. In fact, [4] and [28] used w/c values as high as 1.29 and 0.84, respectively, in their testing program. This encourages the authors to use a higher water content in the mortar mix to imitate the site condition. The current study uses a water to cementitious material ratio (w/cm) of 0.6–0.7, which falls within the recommended boundary [35]. The fresh mortar mix was produced by adding water to the dry mortar mix maintaining a w/cm of 0.6. To study the influence of w/cm on the uniaxial and triaxial behaviour, additional specimens were prepared with a w/cm of 0.7. A total of 90 specimens were prepared for the experimental program; three specimens for each uniaxial loading and triaxial loading conditions were used to capture any strength variation within the samples. To ensure consistency in the preparation, a total of 60 air-dried specimens and 15 wet specimens were prepared from the same batch of mortar with $w/cm = 0.6$, while fifteen specimens with $w/cm = 0.7$ were prepared from a separate batch. The specimens were tested at a curing age of 3, 7, 14, and 28 days, respectively.

A calculated amount of M3 mortar mix and water was added to obtain the desired w/cm as per AS 1012.2 [36]. Two days after casting, the mortar specimens were carefully demoulded and transferred into the curing tank for curing as per AS 1012.8.1 [37]. Each air-dried specimen was taken out of the curing tank and air-dried for approx. 24 h before testing. The wet (fully saturated) specimens, on the other hand, were taken out of the curing tank, dried with a towel, and tested immediately.



2.2 Experimental setup

Since the uniaxial or unconfined compression test is one of the most popular laboratory tests for concrete and mortar [5], these test methods are well established and standardised by several international standards. A separate standard for the triaxial testing of mortar is not available [38]. The triaxial test guideline provided by the RILEM Technical Committee [39] applies to 10 mm thick bed joint mortar specimens only, which can be difficult to obtain in many cases. As such, the previous studies [4, 13–17, 39] investigating the performance of mortar under triaxial loading were consulted while designing this experimental program. Figure 1a, b shows the uniaxial and triaxial test setup used in the experimental program. The test setup consisted of two independently controlled loading components, capable of applying axial load along the ends of the specimen and uniform confining pressure over the specimen's outer surface. The axial load (σ_1) was applied to the ends of the specimen using an upward-moving loading platform, which was attached to a 50 kN hydraulic piston. A vertically positioned load cell was used to record the applied axial load, while a linear variable displacement transducer (LVDT), shown in Fig. 1a, was used to record the axial displacement. A pressure vessel capable of applying 1700 kPa confining pressure, mounted on top of the loading platform, was used to apply the confining pressure (σ_3). De-aired water under pressure, produced with an air compressor, was used to exert the confining pressure on the specimens. A pressure transducer plumbed into the pressure vessel was used to monitor the confining pressure, while a dual automatic pressure controller was used to regulate the confining pressure. The whole setup was assembled in a steel frame. A data acquisition unit interfaced with a dedicated computer was used to apply and record the displacement, axial load, and confining pressure.

The specimens were carefully covered with a thin rubber membrane and connected to the base pedestal and the top cap, as shown in Fig. 1c, to restrict possible water penetration during the triaxial testing. Different axial strain rates were used by researchers in their experimental program; for example, [22] and [13] used a strain rate of 0.007 mm/s (0.42 mm/min) and 0.005 mm/min, respectively. A strain rate of 0.05 mm/min was used in the present study, which

conforms to the test specifications of AS3700 [34] of 0.0005–5 mm/min. While most researchers used a higher magnitude of confining pressure to simulate the triaxial stress state in the mortar (which results in a significant expansion of the failure envelope [27, 28]), this study focuses on the effect of the lower magnitude of confining pressure on the axial compressive strength and failure envelope of mortar. This is more onerous as typical residential masonry structures are not multi-storeyed, hence, a low confining pressure is more realistic. For the uniaxial testing, σ_3 was set to 0 kPa, while for the triaxial testing, σ_3 was set to 100, 250, 500 and 750 kPa, respectively ($\sigma_3/\sigma_1 = 0.016$ –0.12).

In UPV testing, ultrasonic sound waves above 20 kHz frequency are passed through the test specimen. The waves are regulated using a combination of transmitting and receiving transducers. The velocity of the ultrasonic wave passing through the specimen commonly referred to as the UPV depends on the crystal structures, mechanical properties, and defects in the test material. In this study, a Proceq Pundit PL-200 instrument, 54 kHz Proceq transducers and ultrasonic couplant gel were used in the UPV measurement. The UPV test setup was calibrated using a Pundit calibration rod. UPV was measured using the direct transmission method by placing the transmitting and receiving transducers on the opposite sides of the specimen, as shown in Fig. 1d. The UPV measurements were taken using the inbuilt automatic measurement procedure of the Pundit PL-200 instrument. For a comprehensive review of the application and development in the UPV assessment techniques for quasi-brittle materials, readers are encouraged to review the article by Breyse [40]. All the UPV testing was conducted before the destructive testing.

3 Test results and discussion

The test results, i.e., density, stress–strain relationship, Mohr–Coulomb failure envelope, UPV, dynamic modulus of elasticity, strength envelope, influence of saturation and w/cm , the correlation between axial compressive strength and confining pressure and between axial compressive strength and UPV are discussed in this section.



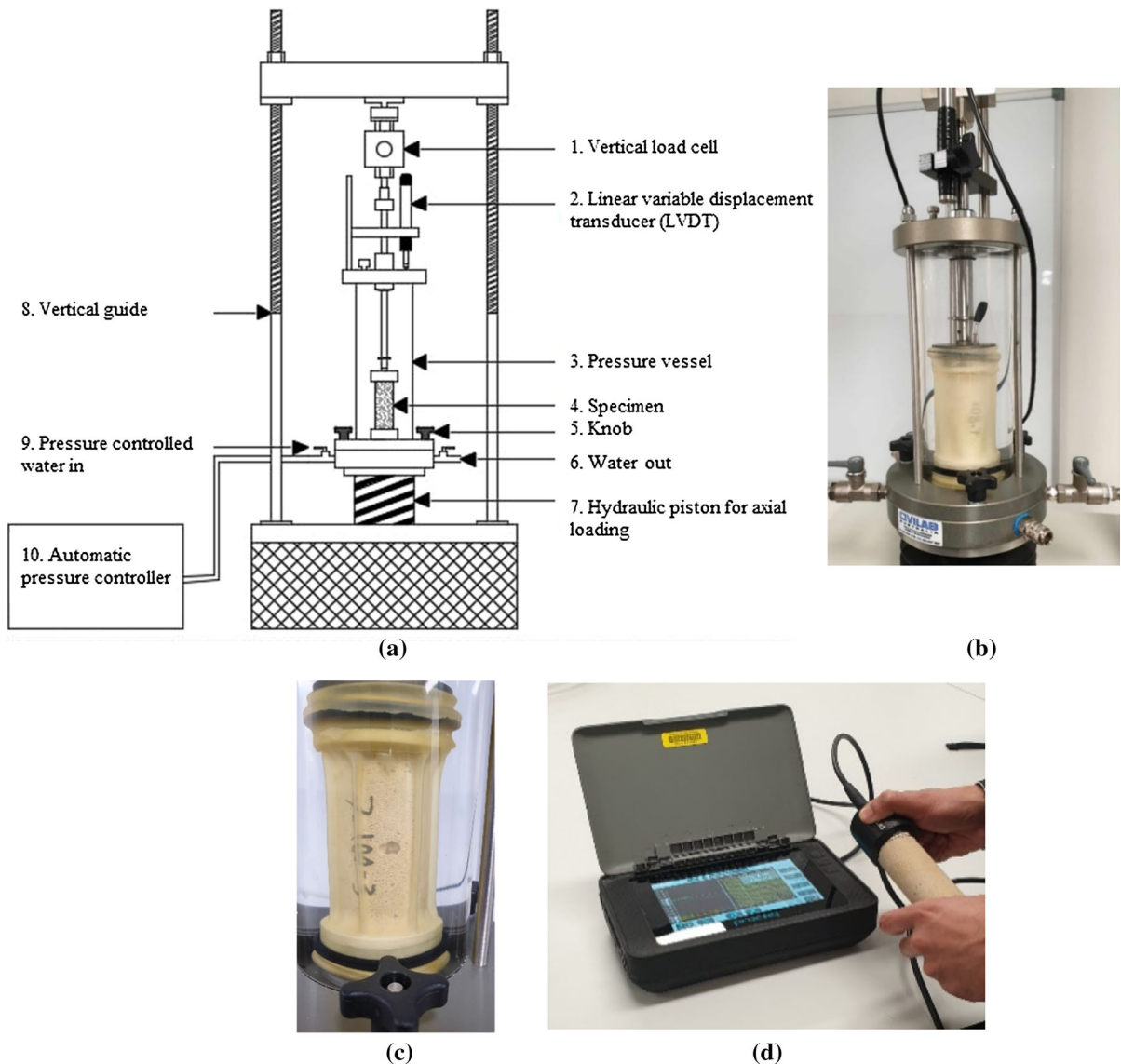


Fig. 1 Experimental details **a** triaxial test setup, **b** test in-progress, **c** rubber membrane fixture, **d** UPV test

3.1 Density

The mass (m) of each specimen was recorded before the destructive testing. The density of the specimen was calculated using Eq. 2, where V is the volume of the specimen.

$$\rho = \frac{m}{V} \quad (2)$$

Figure 2 shows the density of the mortar specimens. It can be seen that the density of the specimens increased with the age of the mortar, which is linked to

the continuing hydration of the cement and lime present in the mortar mix and the subsequent formation of calcium silicate hydrate gel. The average density of the 3, 7, 14, and 28 days specimens were 1834.3, 1869.2, 1885.6 and 1905.6 kg m⁻³, respectively.

3.2 Stress–strain relationship

Figure 3 shows the stress–strain plot of the mortar specimens under uniaxial compression loading. It can be seen that the axial compressive strength (σ_o) of the

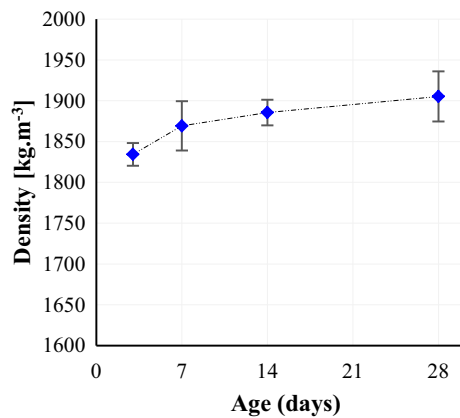


Fig. 2 Density of air-dried mortar specimens with $w/cm = 0.6$

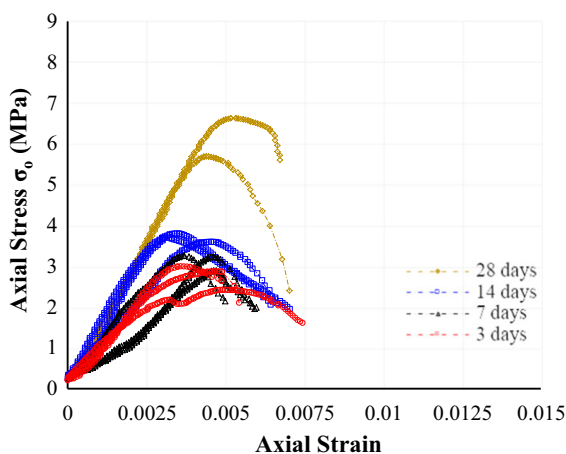


Fig. 3 Axial stress–strain plot of $w/cm = 0.6$ specimens from the uniaxial test

mortar specimens under uniaxial loading increased with the curing age. The average axial compressive strength of the 3, 7, 14, and 28 days specimens was 2.88, 3.01, 3.65 and 6.25 MPa, respectively. A further investigation on the strength values reveals that the 3, 7, and 14 days specimens attained a compressive strength of 43, 45 and 55% of the 28 days compressive strength, respectively. Such behaviour may be due to the high w/cm used in the mix as well as the presence of lime, which contributed through the delayed strength gain mechanism.

Figure 4a, b, c and d shows the axial stress–strain plot of the mortar specimens under triaxial loading with confining pressures of 100, 250, 500, and 750 kPa, respectively. It is clear that the axial compressive strength and shape of the stress–strain

plot is influenced by the presence of confining pressure. Figure 4a shows the stress–strain plot of the 7, 14, and 28 days specimens under a confining pressure of 100 kPa ($\sigma_3/\sigma_1 = 0.016$). Most of these specimens demonstrated a brittle response with steep post-yield softening. Similar to the uniaxial test, the axial compressive strength of the mortar specimens increased with curing age. The average axial compressive strength of the 7, 14, and 28 days specimens was 2.83, 3.69 and 5.55 MPa, respectively. It was also observed that the 3 days specimens struggled through the triaxial testing due to the low compressive strength. Under a confining pressure of 100 kPa, the 3 days old specimens disintegrated at the initiation of the axial load. It was identified that the lower level of confining pressure caused the initial weakening of the specimens. After the initiation of the axial load, the low confining pressure was insufficient in providing lateral support to the specimens to maintain their integrity. It should be noted that the strain of the mortar samples was measured from the LVDT sample deformation data. A direct strain measurement on the material surface was not possible with the current test setup. In the post-processing stage, the data recorded before a proper contact between the specimen and the loading platen was established, has been discarded from the plot, which caused the slight deviation of the first data point from the $x, y = (0, 0)$ point.

The average axial compressive strengths of the 3, 7, 14, and 28 days specimens under a confining pressure of 500 kPa ($\sigma_3/\sigma_1 = 0.08$) were 4.13, 3.91, 5.91, and 7.39 MPa, respectively, as shown in Fig. 4c. The average axial compressive strengths of the 3, 7, 14, and 28 days specimens under a confining pressure of 750 kPa ($\sigma_3/\sigma_1 = 0.12$) were 4.86, 4.95, 6.45, and 8.12 MPa, respectively, as shown in Fig. 4d. It can be seen that the axial stress–strain plot expanded under a confining pressure of 500 and 750 kPa, with any post-yield softening being more subtle, which indicates the effectiveness of the confining mechanism at a confining pressure as low as 500 kPa ($\sigma_3/\sigma_1 = 0.08$). The compressive strength of the mortar specimens also increased with the increase in confining pressure.

Figure 4b shows that the average axial compressive strength of the 3, 7, 14, and 28 days specimens under a confining pressure of 250 kPa ($\sigma_3/\sigma_1 = 0.04$) was 2.9, 3.20, 4.84 and 6.91 MPa, respectively. It was also observed that the axial compressive strength and shape of the stress–strain plot is less influenced by the

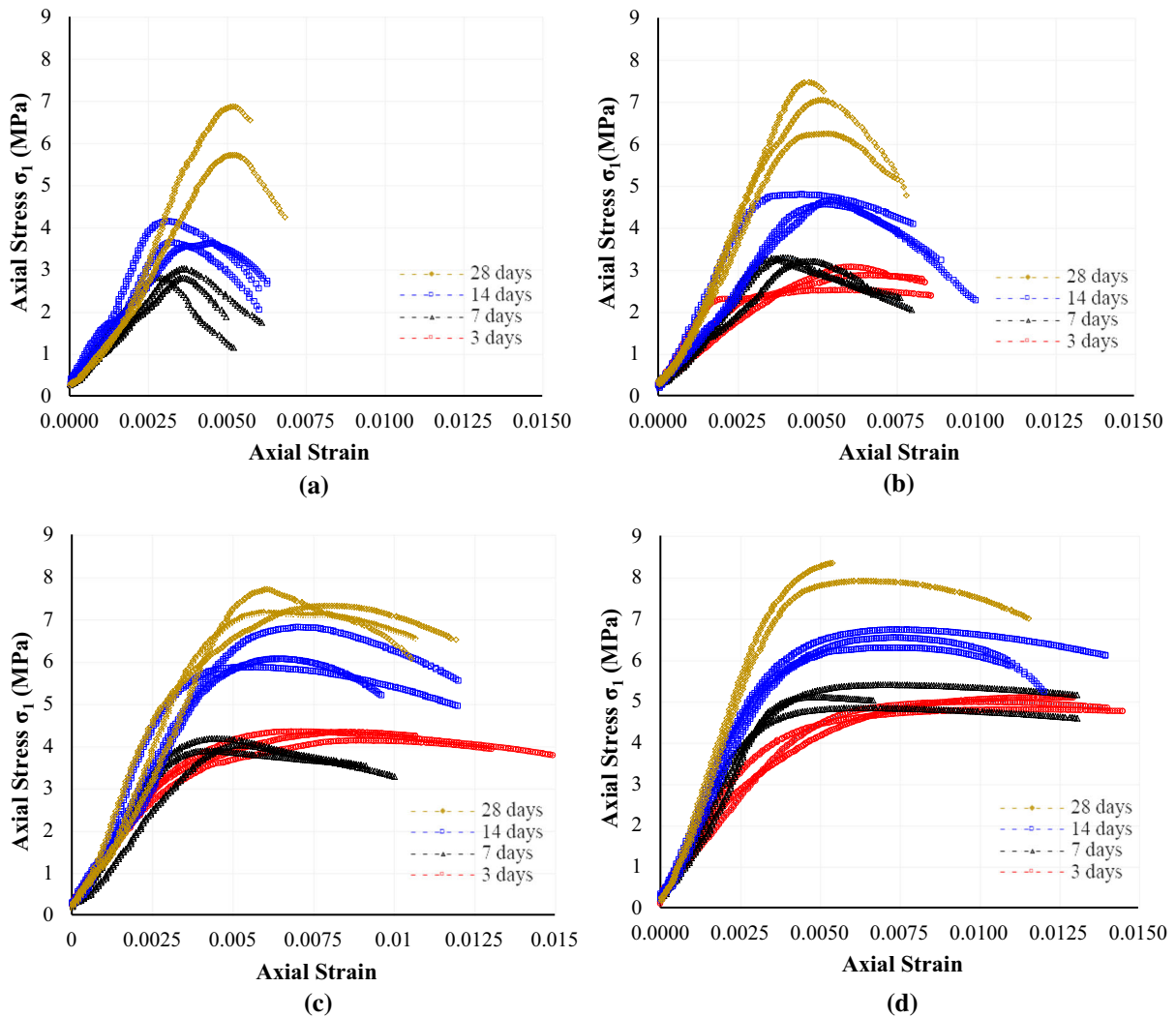


Fig. 4 Axial stress–strain plot of $w/cm = 0.6$ specimens under varying confining pressure **a** 100 kPa; **b** 250 kPa; **c** 500 kPa, **d** 750 kPa

relatively low confining pressures ($\sigma_3/\sigma_1 = 0.016–0.04$). In fact, the stress–strain plot of all the mortar specimens under 100 and 250 kPa confining pressure were similar to those observed in the uniaxial testing shown in Fig. 3.

The compressive fracture energy (G_{fc}) of the mortar specimens was estimated by dividing the area of the absorbed energy of the compressive load–displacement plot with the cross-sectional area of the specimen [41]. G_{fc} of the 28 days specimen under a confining pressure of 0, 100, 250, 500 and 750 kPa were 2.39, 2.71, 5.83, 6.44 and 7.86 Nmm/mm², respectively. The same of the 14 days specimens were 1.44, 1.61, 3.22, 5.45 and 5.72 Nmm/mm², respectively, and

7 days specimens were 0.96, 0.88, 1.74, 2.64 and 5.23 Nmm/mm², respectively. G_{fc} of the 3 days specimen under a confining pressure of 0, 250, 500 and 750 kPa were 1.12, 1.68, 3.49 and 4.75 Nmm/mm², respectively.

Figure 5 shows the average stress–strain plot of the mortar specimens with varying curing ages. Figure 5a, b, c and d shows the stress–strain plot of the 3, 7, 14, and 28 days specimens, respectively. The stress–strain plot expanded with the increase in the confining pressure. From Fig. 5a it can be seen that under a confining pressure of 250, 500 and 750 kPa, the axial compressive strength of the 3 days specimens increased by 0.7, 50.7 and 72.9%, respectively,

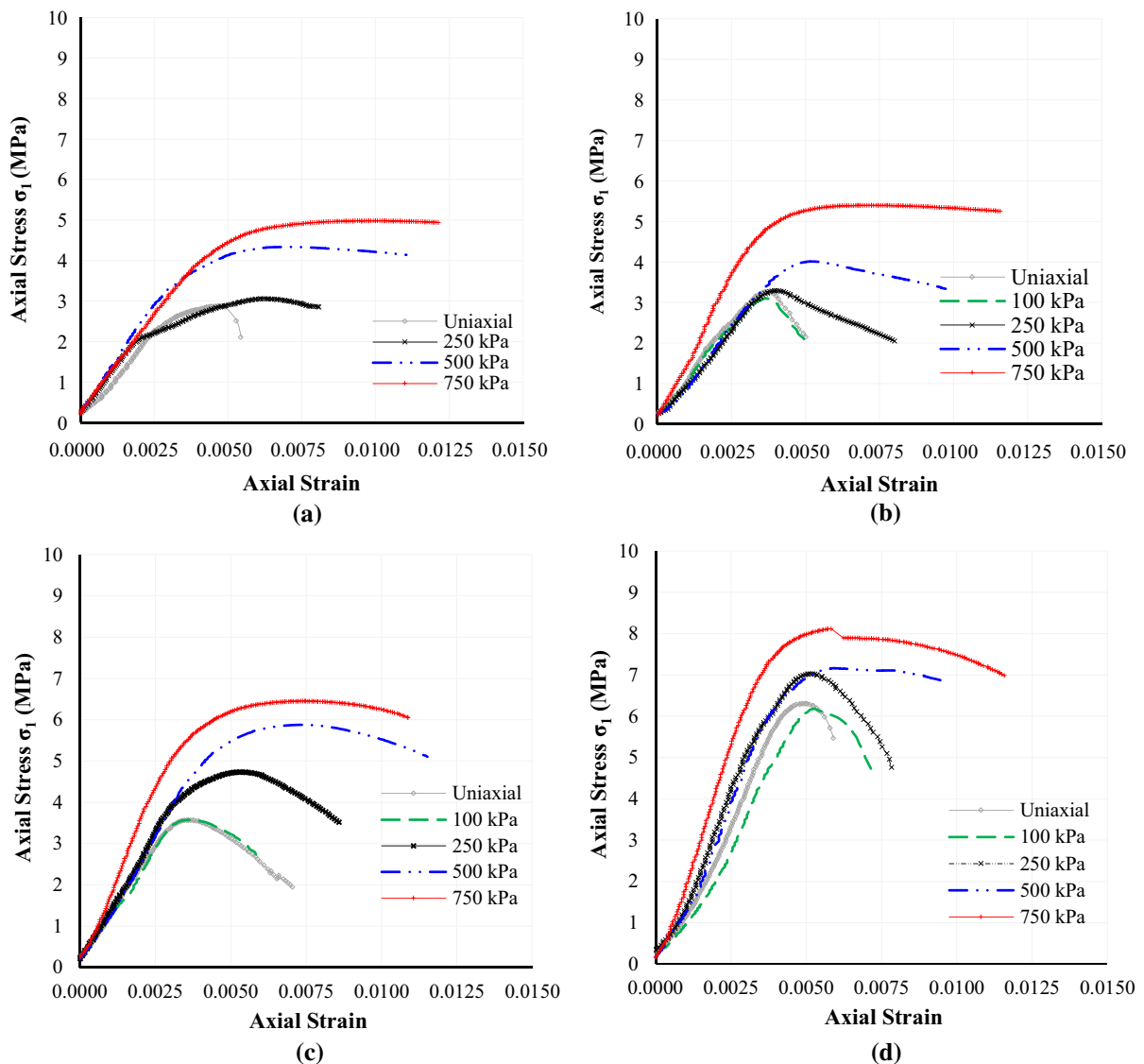


Fig. 5 Effect of curing age on stress–strain response on $w/cm = 0.6$ specimens **a** 3 days; **b** 7 days; **c** 14 days; **d** 28 days

compared to the axial compressive strength obtained in the uniaxial testing. Figure 5b shows that the compressive strengths of the 7 days specimens under a confining pressure of 100, 250, 500 and 750 kPa increased by 1.28, 1.38, 29.1 and 86.5%, respectively. The same for the 14 days specimens increased by 1.19, 39.5, 68.4 and 85.7%, respectively, as shown in Fig. 5c, and that of the 28 days specimens increased by 0.21, 23.7, 25.8 and 40.6%, respectively, as shown in Fig. 5d. The shape of the stress–strain plot also changed with varying levels of confining pressure.

Figure 5 further reveals that under pure uniaxial loading conditions (zero confining pressure), the specimens showed a brittle behaviour with a sharp decrease in strength in the post-peak zone. With an increase in the confining pressure, the commercial mortar specimens demonstrated more ductility in the post-peak softening zone, which is consistent with the previous studies reported in [4, 27, 28]. All the specimens under relatively higher confining pressures of 500 and 750 kPa showed more ductile behaviour with only a subtle drop in the compressive stress even under higher axial strain levels. Similar behaviour was

also observed by Toufigh et al. [22], Wang et al. [26] and Atkinson et al. [28].

3.3 Failure mode

Figure 6 shows the failure mode of the mortar specimens. Figure 6a and b shows the 28 days test specimens before and after the triaxial testing, respectively. A typical shear failure at an angle of about 45 degrees was observed in the triaxial test, as shown in Fig. 6b, which also matches the failure modes reported in [22].

3.4 Mohr–Coulomb envelope

A series of Mohr circles were drawn for each group of specimens (for varying curing age, wet/air-dry condition and varying $w/cm = 0.6$ and 0.7), where each Mohr-circle was obtained using a specific σ_3 and the corresponding σ_1 value (Fig. 7). The tensile strength of mortar f_t was obtained using the correlation $f_t = 0.3 \sigma_0$. This equation was proposed in [1, 11] based on an extensive experimental program on a similar type of mortar. The shear strength parameters c and ϕ of the specimen were derived by drawing a tangent to all the Mohr circles of a particular group of specimens. c of the specimen was obtained from the intersection point between the tangent and the $\sigma = 0$ line, while the ϕ of the specimen was obtained from the slope of the tangent. The shear strength for each

group of specimens was calculated from the Mohr–Coulomb failure envelope equation given in Eq. 1.

Figure 7a, b, c and d shows the Mohr circles along with the Mohr–Coulomb failure envelope of the 3, 7, 14 and 28 day air-dried mortar specimens, respectively. Figure 7e and f shows the Mohr circles along with the Mohr–Coulomb failure envelope of the mortar specimens in the wet condition with $w/cm = 0.6$ and in the air-dried condition with $w/cm = 0.7$, respectively. The Mohr–Coulomb failure envelope, cohesion and angle of internal friction of the specimens are presented in Table 1. It can be seen that the c and ϕ values and the failure envelope changed with changes in the curing age. In particular, the c value gradually increased with an increase in curing age. This can be linked to the progressive formation of the hydration products of the cement paste [13] that resulted in higher bond strength between the matrix of the mortar and provided a higher compressive strength to the older specimens. The c values of the 3, 7, 14 and 28 days mortar specimens was 0.781, 0.911, 1.07 and 1.503 MPa, respectively, which falls within the c value of 0.28–4.76 MPa [42] and 2.30 MPa [43] obtained for mortar. On the other hand, the ϕ value was less influenced by the curing age and varied within the range of 32–33°

For a comprehensive understanding of the influence of wet conditions and the w/cm on the Mohr–Coulomb failure envelope, the results of the 28 days air-dry samples with $w/cm = 0.6$ are plotted parallelly in Fig. 7e and f. It can be seen that both the wet and dry conditions and the w/cm impacted the c and ϕ values. The c value of the wet specimens and the $w/cm = 0.7$ specimens were 1.175 and 0.371 MPa, respectively, which is 21.8 and 75.3% lower, respectively than the 28 days air-dry specimen with $w/cm = 0.6$.

3.5 UPV and dynamic modulus of elasticity

Figure 8 shows the UPV and dynamic modulus of elasticity (E_{dyn}) of the tested mortar specimens. The UPV of each specimen, shown in Fig. 8, is the average value of three independent readings taken along the axial direction of the specimen. E_{dyn} was calculated as per the procedure outlined in [11], using Eq. 3.

$$E_{dyn} = 0.001 \times \rho \times UPV^2 \quad (3)$$



Fig. 6 Triaxial test specimen **a** before testing (top row), **b** after testing (bottom row)

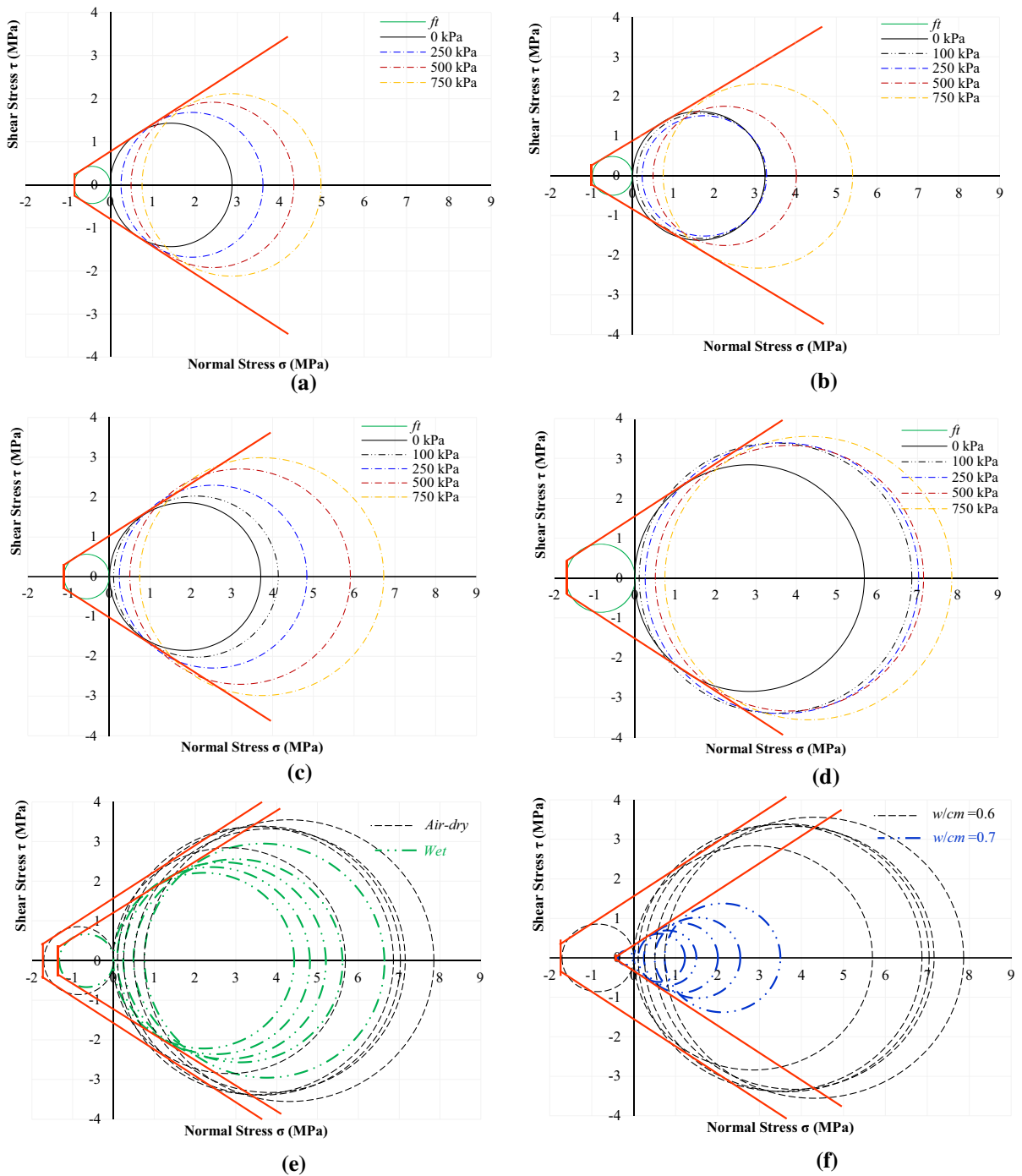


Fig. 7 Mohr circle of mortar **a** 3 days, **b** 7 days, **c** 14 days, **d** 28 days, **e** wet condition, **f** $w/cm = 0.6$ and 0.7

where ρ is the density of the mortar specimen in $g \cdot cm^{-3}$, obtained from Sect. 3.1.

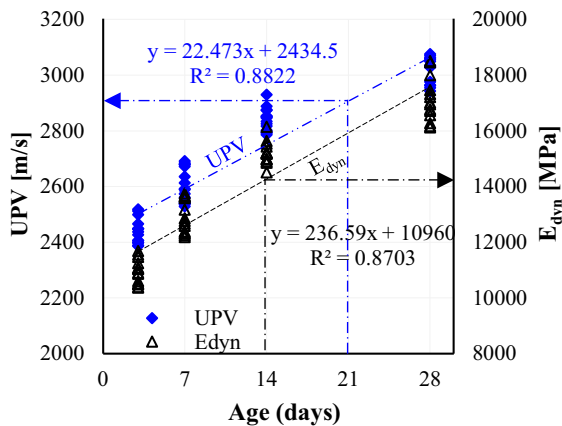
From Fig. 8, it is clear that the UPV readings increased with the curing age. Such changes can be

linked to the changes in the crystal structure of the specimen, which is a consequence of the ongoing hydration process of the cement lime mortar. The average UPV of the 3, 7, 14, and 28 days specimens



Table 1 Shear strength and failure MC failure envelope of commercial cement lime mortar

Curing age	Testing condition	w/cm	Cohesion <i>c</i> (MPa)	Angle of internal friction φ (°)	Failure envelope
3 days	Air-dry	0.6	0.781	33	$\tau = 0.781 + 0.649 \sigma$
7 days			0.911	32	$\tau = 0.911 + 0.625 \sigma$
14 days			1.071	33	$\tau = 1.071 + 0.649 \sigma$
28 days			1.503	33	$\tau = 1.503 + 0.649 \sigma$
28 days	Wet		1.175	32	$\tau = 1.175 + 0.625 \sigma$
28 days	Air-dry	0.7	0.371	33	$\tau = 0.371 + 0.649 \sigma$

**Fig. 8** Changes in UPV and E_{dyn} with curing age

were 2438 ± 44 , 2607 ± 61.3 , 2848 ± 49.6 and 3018 ± 48.2 m/s, respectively. The average E_{dyn} of the 3, 7, 14, and 28 days specimens were $10,911 \pm 436$, $12,909 \pm 596$, $15,189 \pm 384$ and $17,102.5 \pm 778$ MPa, respectively. Based on the UPV and E_{dyn} measurements, a linear correlation between UPV and curing age, and between E_{dyn} and curing age was established. These are shown in Eqs. 4 and 5, with $R^2 = 0.88$ and $R^2 = 0.87$, respectively. These equations can help estimate the mechanical properties of mortar.

$$UPV = 22.473t + 2434.5 \quad (4)$$

$$E_{dyn} = 236.6t + 10960 \quad (5)$$

where t is the curing age of the specimen in days.

3.6 Strength envelope

Figure 9a, b, c and d shows the axial strength versus confining pressure plot of the 3, 7, 14, and 28 days specimens, respectively. The graph is obtained by

plotting the maximum axial compressive stress (σ_1) of each specimen against the respective applied confining pressure (σ_3). The strength envelope was developed by using the linear correlation between the axial compressive strength of mortar of each age group and the applied confining pressure. The correlations developed for the 3, 7, 14, and 28 days specimens are given in Eqs. 6, 7, 8 and 9, respectively, with R^2 values of 0.82, 0.91, 0.86 and 0.71, respectively. The strength envelope developed for the commercial mortar were consistent with those proposed in [4, 28], as discussed later. The relatively low regression coefficient for the 28 days specimens is due to the scatter in the measurements at low confining pressure levels. More statistical analyses on all fitted equations are presented later.

$$\sigma_{1(3)} = 0.0033 \sigma_3 + 2.35 \quad (6)$$

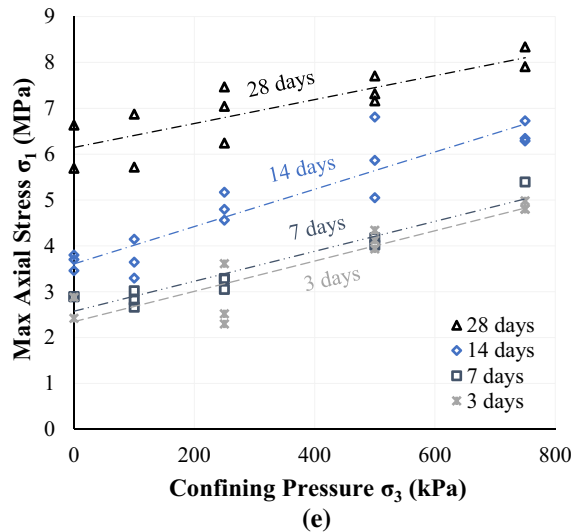
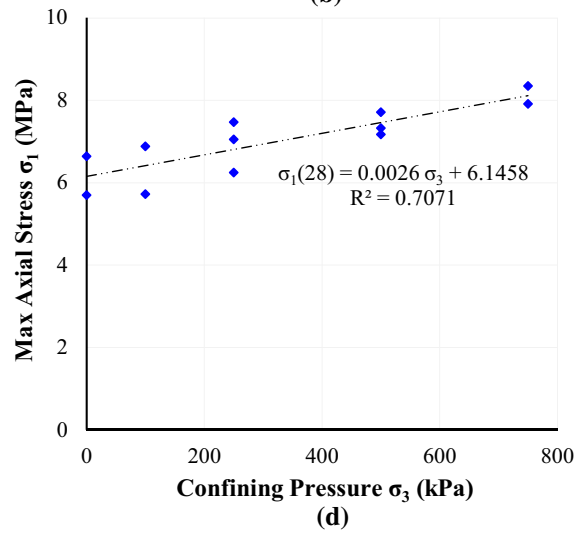
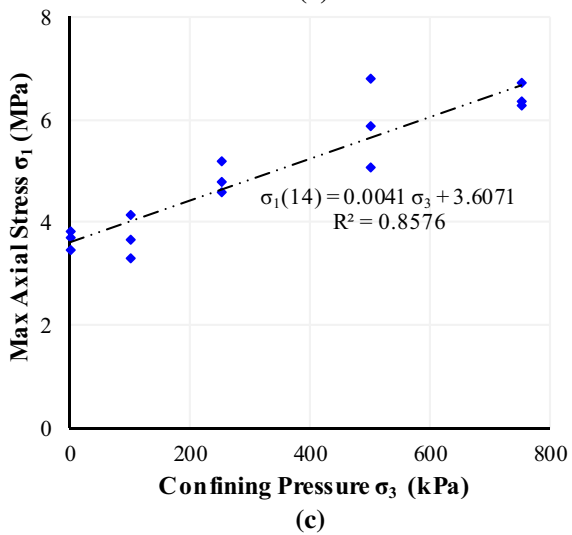
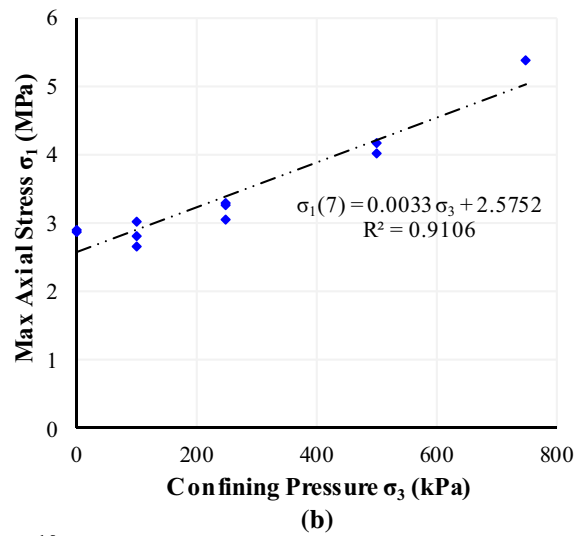
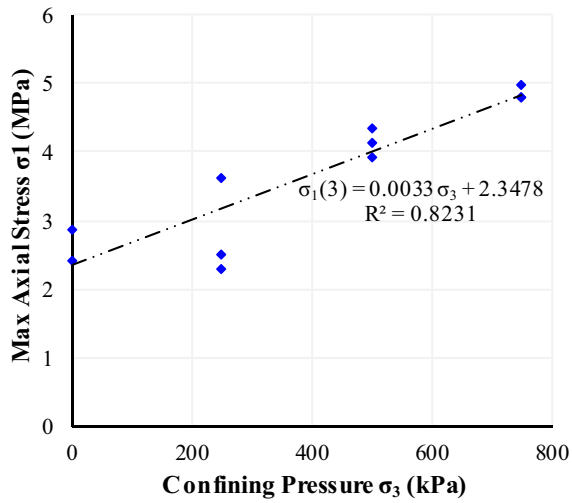
$$\sigma_{1(7)} = 0.0033 \sigma_3 + 2.58 \quad (7)$$

$$\sigma_{1(14)} = 0.0041 \sigma_3 + 3.61 \quad (8)$$

$$\sigma_{1(28)} = 0.0026 \sigma_3 + 6.10 \quad (9)$$

where, ($\sigma_{1(x)}$) is the major principal stress (axial compressive strength) in MPa, x is the age of the specimen in days and (σ_3) is the minor principal stress (confining pressure) in kPa. This relation can be practically useful in estimating the axial compressive strength of mortar subjected to varying levels of confining pressure.

Figure 9e shows the strength envelope of mortar of different age groups plotted parallel to each other. A slight change in the slope of the strength envelope could be observed due to changes in the curing age. It was also observed that the strength envelope expanded with the curing age. The 3 days specimens had the



◀ **Fig. 9** Strength envelope **a** 3 days; **b** 7 days; **c** 14 days; **d** 28 days; **e** combined

smallest (lowest) strength envelope whereas the 28 days specimens had the largest (highest) strength envelope.

From a practical point of view, testing individual mortar specimens in a laboratory under different confining pressures can be a time consuming and expensive task. The correlations developed in this paper can help in quickly estimating the axial compressive strength of mortar under varying confining pressures.

3.7 Air-dried vs wet specimen

Figure 10 shows the strength envelope of the air-dried and wet mortar specimens. A set of 15 additional 28 days wet specimens were tested to create the wet dataset. The linear correlation between the peak axial compressive strength and confining pressure, shown in Eq. 10, is used to develop the strength envelope of the wet specimens. The strength envelope of the 28 days air-dried (dry) specimens, shown in Eq. 8, is also plotted to better understand the performance of wet/saturated mortar under triaxial loading.

$$\sigma_{1(28)\text{wet}} = 0.0015 \sigma_3 + 4.45 \quad (10)$$

where $\sigma_{1(28)\text{wet}}$ is the major principal stress (axial compressive strength) of the 28 days wet specimens.

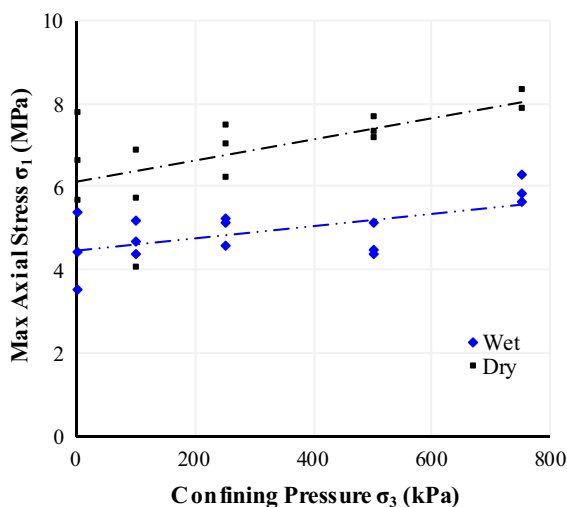


Fig. 10 Strength envelope for dry and wet 28 days specimen

From Fig. 10, it can be seen that the position of the strength envelope of the wet specimens is lower than the dry specimens. This is due to the comparatively lower axial compressive strength of the wet specimens. The strength envelope of both the wet and dry specimens demonstrated certain parallelism.

3.8 Influence of w/cm ratio

Figure 11 shows the influence of w/cm on the axial compressive strength of mortar specimens under varying levels of confining pressure. Figure 11a and b shows the stress–strain plot and strength envelope, respectively, of mortar specimens with $w/cm = 0.6$ and $w/cm = 0.7$.

From Fig. 11a, it can be seen that the axial compressive strength of the $w/cm = 0.7$ specimens is noticeably lower than the $w/cm = 0.6$ specimens, which is due to the excessive water content in the $w/cm = 0.7$ mixture [5]. The average axial compressive strength (σ_o) of the $w/cm = 0.7$ specimens obtained from the uniaxial testing was only 16.5% of that of the $w/cm = 0.6$ specimens. The stress–strain plots of the $w/cm = 0.7$ specimens also expanded with the increase in confining pressure, although they are distinctively lower than the $w/cm = 0.6$ specimens. Under a confining pressure of 100, 250, 500 and 750 kPa, the axial compressive strengths of the $w/cm = 0.7$ specimens were just 22.5, 27.2, 27.6 and 31.5%, respectively, of that of the $w/cm = 0.6$ specimens. From visual observation of the plots, it is apparent that the modulus of elasticity of the $w/cm = 0.7$ specimens is much lower than the $w/cm = 0.6$ specimens. This suggests that $w/cm = 0.7$ will result in a poor-quality mortar using the commercial mortar mix. Under a confining pressure of 100, 250, 500 and 750 kPa, the average axial compressive strengths of $w/cm = 0.7$ specimens were 1.25, 1.88, 2.04 and 2.57 MPa, respectively.

Figure 11b shows the strength envelope of the $w/cm = 0.6$ and $w/cm = 0.7$ specimens. It is clear that the strength envelope of the $w/cm = 0.7$ specimens is lower than the $w/cm = 0.6$ specimens. A linear correlation between the axial compressive strength and confining pressure of the $w/cm = 0.7$ specimens could be established with an R^2 value of 0.92, which is shown in Eq. 11.

$$\sigma_{1(28)w/cm=0.7} = 0.0015 \sigma_3 + 4.45 \quad (11)$$

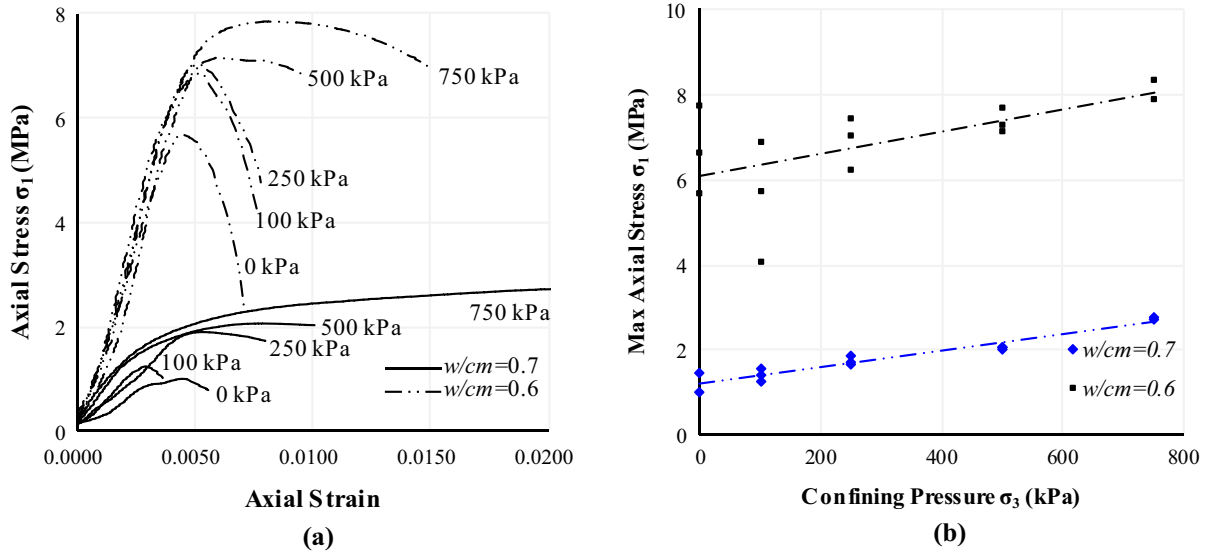


Fig. 11 Influence of w/cm on axial compressive strength **a** stress–strain plot, **b** strength envelope

where $\sigma_{1(28)w/cm=0.7}$ is the 28 days axial compressive strength of mortar specimens with $w/cm = 0.7$

The correlation between peak stress and confining pressure for samples of all curing ages, curing conditions and w/cm 's are shown in Fig. 12.

From Fig. 12, it is seen that the mortar specimens experienced an increase in the axial compressive strength along with an increase in the level of confining pressure. Although the correlations demonstrated parallelism, the slope of the fitted line of the wet specimens was comparatively lower than the slope of all the other dry specimens. This indicates that the

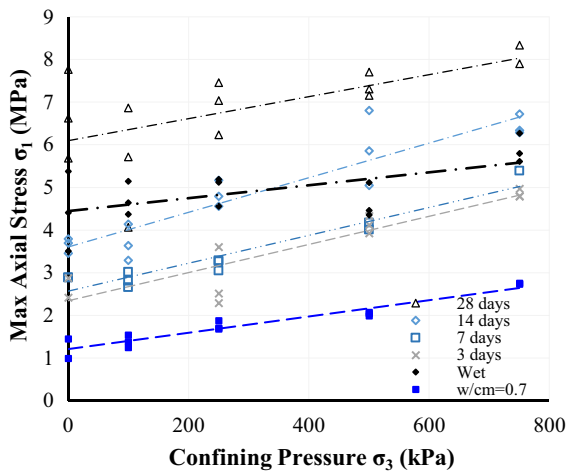


Fig. 12 Strength envelope of all tested specimens

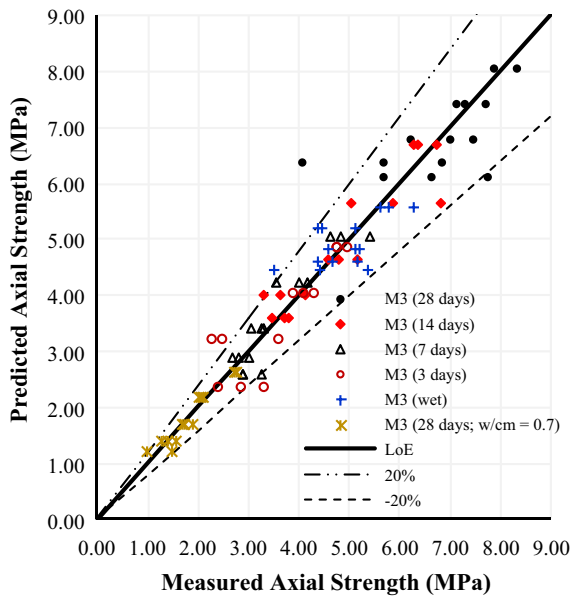


rate of increase in the axial compressive strength of the wet specimens with an increase in the confining pressure was lower than similar dry specimens. Such a behaviour of the wet specimens can be associated with the pore pressure effect; similar behaviour has been reported by Vu et al. [44] for concrete with a higher degree of saturation.

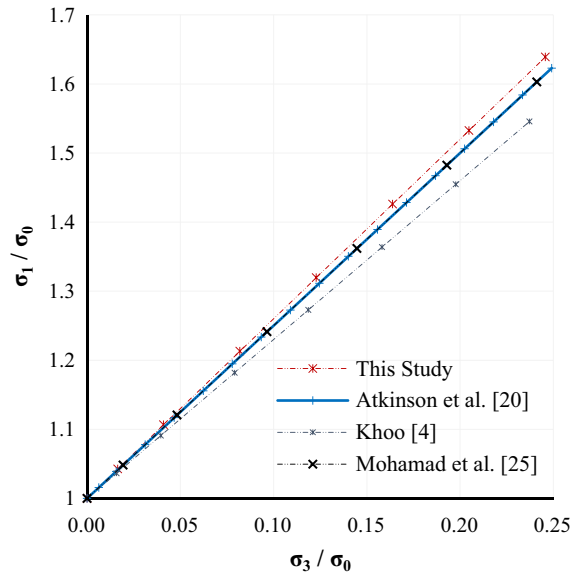
3.9 Analysis of test data

Figure 13a shows the axial compressive strength plot of the mortar specimens predicted using Eqs. 6–11 against the experimental predictions. It is seen that most of the experimental data fall within $\pm 20\%$ bounds from the line of equality (LoE). The mean measured over predicted ratio is essentially unity (~ 1), with a low coefficient of variation (CoV) and standard deviation (SD) of 0.12.

Figure 13b shows a comparison of the strength envelope proposed in Eq. 9, with strength envelopes of 28 days old masonry mortar of similar composition taken from the literature [4, 17, 28]. It is seen that the proposed strength envelope for the commercial mortar with a high w/cm of 0.6–0.7 closely match the strength envelope proposed in [28] and [17], which affirms the suitability of the mortar for masonry construction. It is also observed that the strength envelope proposed in Eq. 9 varied the most with the strength envelope proposed in Khoo [4]. This may be due to the quality



(a)



(b)

Fig. 13 Performance of test data, **a** predicted vs measured strength of all uniaxial and triaxial tests (total data points 84), **b** performance of strength envelope

of the constituents of the commercial mortar and the high w/cm used in the present study.

3.9.1 Correlation between UPV and axial compressive strength

As already discussed in the previous sections, the axial compressive strength of the mortar specimens can be estimated by means of pulse velocity. The relation between σ_o (obtained from the uniaxial testing) and the UPV measurements (along the axial direction of the specimen) is shown in Fig. 14a. A linear correlation between σ_o and UPV is established, as shown in Fig. 14a, and Eq. 12, with $R^2 = 0.72$. This correlation can be used to estimate the axial compressive strength of mortar under uniaxial loading from the measured UPV values.

$$\sigma_o = 0.0055 \text{ UPV} - 10.93 \tag{12}$$

Figure 14b–e shows the axial compressive strength (σ_1) of the mortar specimens obtained from the triaxial testing plotted against the respective UPV measurements. As discussed earlier, the UPV measurements were taken before the triaxial testing. Since the UPV was measured along the axial direction of the specimen, which is also the direction of the axial

compression loading, the UPV could not be simultaneously measured during the triaxial testing.

Figure 14b, c, d and e shows the σ_1 versus UPV plot of the mortar specimens subjected to a confining pressure of 100, 250, 500 and 750 kPa, respectively. A linear correlation between σ_1 and UPV is established for each set of confining pressure. The correlations for confining pressures of 100, 250, 500 and 750 kPa are given in Eqs. 13, 14, 15 and 16, respectively, with R^2 values of 0.61, 0.91, 0.85 and 0.78, respectively.

$$\sigma_{1(100)} = 0.0062 \text{ UPV} - 13.28 \tag{13}$$

$$\sigma_{1(250)} = 0.0071 \text{ UPV} - 14.88 \tag{14}$$

$$\sigma_{1(500)} = 0.0059 \text{ UPV} - 10.79 \tag{15}$$

$$\sigma_{1(750)} = 0.0051 \text{ UPV} - 7.97 \tag{16}$$

Figure 14f shows the correlations between σ_1 measured under varying confining pressures and UPV. It can be seen that there is certain parallelism, in that the correlation gradually increased with an increase in the applied confining pressure level. From a practical point of view, the developed correlations presented in Eqs. 13–16 can be particularly useful in predicting the axial compressive strength of mortar

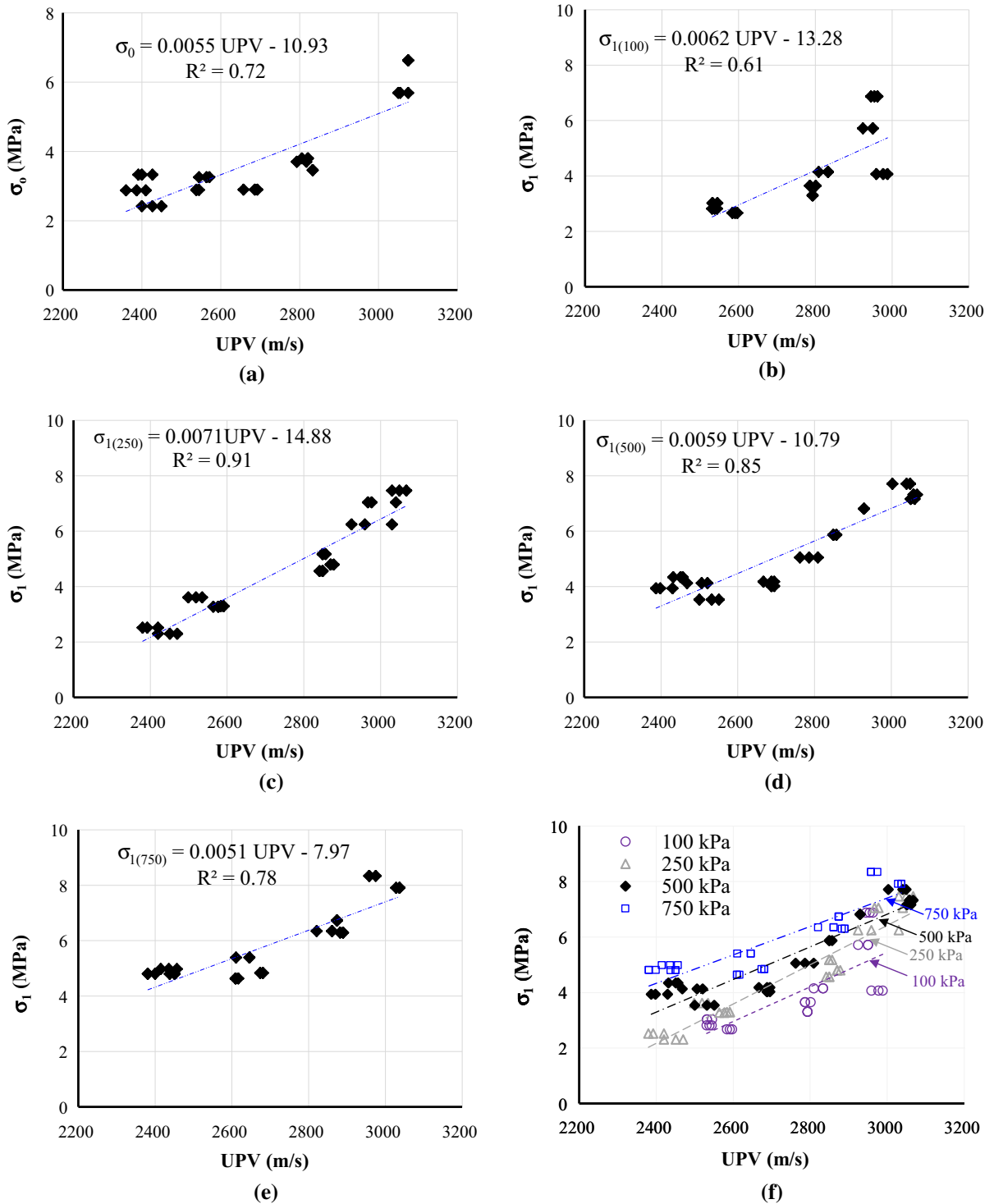


Fig. 14 Correlation between axial compressive strength and UPV under confining pressure **a** 0 kPa, **b** 100 kPa, **c** 250 kPa, **d** 500 kPa, **e** 750 kPa, **f** combined



under triaxial loading from the measured UPV values, without performing the complex triaxial testing.

4 Conclusion

The mechanical properties of a commonly used and commercially available Australian cement-lime masonry mortar under uniaxial and triaxial loading are investigated. A total of 90 cylindrical mortar specimens were tested at curing ages of 3, 7, 14, and 28 days. The water to cementitious material ratio (w/cm) was varied between 0.6 and 0.7. The tests were performed under confining pressures of 100, 250, 500 and 750 kPa. The density, stress–strain curves, UPV, dynamic modulus of elasticity, strength envelope, parameters of Mohr–Coulomb failure envelope, correlations between axial compressive strength and confining pressure, and axial compressive strength and UPV of the mortar specimens were established. The following conclusions are drawn from the research:

- The strength envelope developed for the commercial mortar mix is consistent with mortar of similar composition reported in the literature, which affirms the suitability of the commercial mortar for masonry construction. However, the high w/cm of 0.6–0.7 resulted in relatively low compressive strength. The average uniaxial compressive strength of 28 days old mortar was 6.25 MPa.
- The axial compressive strength of all the 3, 7, 14, and 28 days specimens increased with an increase in the applied confining pressure. Under confining pressures of 100, 250, 500 and 750 kPa the axial compressive strength of the 28 days mortar specimens increased by 0.21, 23.7, 25.8 and 40.6%, respectively.
- The Mohr–Coulomb strength parameters cohesion (c) and friction angle (φ) are affected by the curing age, sample condition (air-dried/wet) and w/cm . c increases with the curing age and the 28 days c value are nearly double the 7 days c value. The wet specimens showed a lower c value compared to the air-dry specimens. The friction angle is less influenced by these parameters and was found to be within the range of 32–33 degrees.
- UPV and E_{dyn} linearly vary with the curing age; the relevant correlations can be useful in predicting the mechanical properties of the mortar.
- Despite some scatter within the data at low confining pressures, the strength envelopes of the mortar specimens may be represented by linear correlations between the axial compressive strength and the confining pressure. The correlations allow a quick estimation of the compressive strength of mortar subjected to varying levels of confining pressure. Using such linear correlations, the compressive strength of all 90 samples tested was shown to be predicted with an accuracy of 20%. The linear correlations, in general, were consistent with other published correlations found in the literature.
- Linear correlations between axial compressive strength obtained from the uniaxial and triaxial testing and UPV have been established. The correlations can be useful in predicting the axial compressive strength of mortar from the measured UPV without physically performing the complex uniaxial and triaxial testing. The correlations between axial compressive strength from triaxial testing and UPV demonstrated certain parallelism despite changes in the applied confining pressure.
- The w/cm ratio has a profound impact on the axial compressive strength of commercial mortar. By increasing the w/cm from 0.6 to 0.7, the compressive strength of the 28 days specimens was reduced by $\sim 70\%$. It was found that the $w/cm = 0.7$ produced a poor-quality mortar with very low compressive strength. The slope of the strength envelope of the $w/cm = 0.7$ specimens was parallel to the $w/cm = 0.6$ specimens, suggesting a similar rate of strength increase with the increasing confining pressure.
- The proposed correlations are best suited for the commercial M3 type mortar, which is widely used by the masonry industry.
- Under relatively low confining pressures (< 500 kPa), the mortar demonstrated brittle behaviour with a sharp post-peak softening response similar to uniaxial testing. Confining pressures beyond 500 kPa were deemed effective in providing lateral confinement, which was demonstrated through the expansion of the stress–strain plot, the transition from brittle to

ductile and the enhanced axial compressive strength.

- The failure of the specimens was characterised by a shear plane developed at $\sim 45^\circ$ with respect to the horizontal plane.
- There is scope to further correlate and enhance the strain measurements made with surface strain measurements with improved apparatus as well as using digital image correlation.

Acknowledgements The authors acknowledge the experimental support provided by Dr Andrei Costache and CQUniversity.

Funding Open Access funding enabled and organized by CAUL and its Member Institutions.

Declarations

Conflict of interest There is no known competing financial interest associated with this publication. There is no other person who satisfied the criteria for authorship but is not listed.

Open Access This article is licensed under a Creative Commons Attribution 4.0 International License, which permits use, sharing, adaptation, distribution and reproduction in any medium or format, as long as you give appropriate credit to the original author(s) and the source, provide a link to the Creative Commons licence, and indicate if changes were made. The images or other third party material in this article are included in the article's Creative Commons licence, unless indicated otherwise in a credit line to the material. If material is not included in the article's Creative Commons licence and your intended use is not permitted by statutory regulation or exceeds the permitted use, you will need to obtain permission directly from the copyright holder. To view a copy of this licence, visit <http://creativecommons.org/licenses/by/4.0/>.

References

- Noor-E-Khuda S, Albermani F (2019) Mechanical properties of clay masonry units: destructive and ultrasonic testing. *Constr Build Mater* 219:111–120
- Page A (2012) The evolution of the design and construction of masonry buildings in Australia. *Gestão Tecnol Proj* 7(2):27–34
- McNary WS, Abrams DP (1985) Mechanics of masonry in compression. *J Struct Eng (ASCE)* 111(4):857–870
- Khoo CL (1972) Failure criterion for brickwork in axial compression. Ph.D. Thesis, University of Edinburgh, Edinburgh
- Haach VG, Vasconcelos G, Lourenço PB (2011) Influence of aggregates grading and water/cement ratio in workability and hardened properties of mortars. *Constr Build Mater* 25:2980–2987
- Asad M, Dhanasekar M, Zahra T, Thambiratnam D (2019) Characterisation of polymer cement mortar composites containing carbon fibre or auxetic fabric overlays and inserts under flexure. *Constr Build Mater* 224:863–879
- de Oliveira TF, Beck MH, Escosteguy PV, Bortoluzzi EC, Modolo ML (2015) The effect of the substitution of hydrated lime with phyllite on mortar quality. *Appl Clay Sci* 105:113–117
- Lanas J, Sirera R, Alvarez JI (2006) Study of the mechanical behavior of masonry repair lime-based mortars cured and exposed under different conditions. *Cem Concr Res* 36(5):961–970
- Singh SB, Munjal P, Thammishetti N (2015) Role of water/cement ratio on strength development of cement mortar. *J Build Eng* 4:94–100
- Binder E, Reihnsner R, Yuan Y, Mang HA, Pichler BLA (2020) High-dynamic compressive and tensile strength of specimens made of cementitious materials. *Cem Concr Res* 129:105890
- Noor-E-Khuda S (2021) Influence of wetting–drying cycles on compressive and flexural strength of cement mortar and CFRP-mortar bond strength. *Constr Build Mater* 271:121513
- Zhou Q, Wang F, Zhu F, Yang X (2017) Stress–strain model for hollow concrete block masonry under uniaxial compression. *Mater Struct* 50(2):106
- Assaad J, Harb J, Khayat K (2009) Use of triaxial compression test on mortars to evaluate formwork pressure of self-consolidating concrete. *ACI Mater J* 106(5):439–447
- Yankelevsky DZ, Karinski YS, Zhutovsky S, Feldgun VR (2018) High-pressure uniaxial confined compression tests of mortars. *Constr Build Mater* 165:523–532
- Yurtdas I, Burlion N, Skoczylas F (2004) Triaxial mechanical behaviour of mortar: Effects of drying. *Cem Concr Res* 34(7):1131–1143
- Yurtdas I, Peng He, Burlion N, Skoczylas F (2006) Influences of water by cement ratio on mechanical properties of mortars submitted to drying. *Cem Concr Res* 36(7):1286–1293
- Mohamad G, Fonseca FS, Roman HR, Vermeltoft A and Rizzatti E (2015) Behavior of mortar under multi-axial stress. In: 12th North American Masonry conference, 17–20 May 2015, Denver, Colorado pp 1–12
- Lourenço PB (1996) Computational strategies for masonry structures. Ph.D. Thesis, Delft University of Technology, Delft
- Noor-E-Khuda S, Dhanasekar M, Thambiratnam DP (2016) Out-of-plane deformation and failure of masonry walls with various forms of reinforcement. *Compos Struct* 140:262–277
- Noor-E-Khuda S (2021) An explicit finite-element modeling method for masonry walls using continuum shell element. *J Archit Eng* 27(4):04021040
- Gabet T, Malécot Y, Daudeville L (2008) Triaxial behaviour of concrete under high stresses: influence of the loading path on compaction and limit states. *Cem Concr Res* 38(3):403–412
- Toufigh V, Abyaneh MJ, Jafari K (2017) Study of behavior of concrete under axial and triaxial compression. *ACI Mater J* 114(4):619–629



23. Sfer D, Carol I, Gettu R, Etse G (2002) Study of the behavior of concrete under triaxial compression. *J Eng Mech* 128(2):156–163
24. Malecot Y, Zingg L, Briffaut M, Baroth J (2019) Influence of free water on concrete triaxial behavior: the effect of porosity. *Cem Concr Res* 120:207–216
25. Chen D, Yu X, Liu R, Li S, Zhang Y (2019) Triaxial mechanical behavior of early age concrete: experimental and modelling research. *Cem Concr Res* 115:433–444
26. Wang YB, Liew JY, Lee SC, Xiong DX (2016) Experimental study of ultra-high-strength concrete under triaxial compression. *ACI Mater J*. <https://doi.org/10.14359/51688071>
27. Hayen R, Schueremans L, Van Balen K, Van Gemert D (2001) Triaxial testing of historic masonry, test set-up and first results. *WIT Trans Built Environ* 55:1–10
28. Atkinson RH, Noland JL, Abrams DP, McNary S (1985) Deformation failure theory for stack-bond brick masonry prisms in compression. In: Mathys JH, Borchelt JG (eds) *Proceedings of 3rd North American Masonry conference*, Arlington
29. Sbartai ZM, Breyse D, Larget M, Balaýssac JP (2012) Combining NDT techniques for improved evaluation of concrete properties. *Cem Concr Compos* 34(6):725–733
30. Sharma S, Mukherjee A (2015) Monitoring freshly poured concrete using ultrasonic waves guided through reinforcing bars. *Cem Concr Compos* 55:337–347
31. Carette J, Staquet S (2016) Monitoring and modelling the early age and hardening behaviour of eco-concrete through continuous non-destructive measurements: part II. *Mech Behav Cem Concr Compos* 73:1–9
32. Noor-E-Khuda S, Albermani F (2019) Flexural strength of weathered granites under wetting–drying cycles: implications to steel structures. *Adv Steel Constr* 15(3):225–231
33. Noor-E-Khuda S, Albermani F, Veidt M (2017) Flexural strength of weathered granites: influence of freeze and thaw cycles. *Constr Build Mater* 156:891–901
34. AS 3700 (Australian Standard) (2018) Australian Standard of Masonry Structures. Sydney
35. Think Brick Australia, Manual To Construction Guidelines for Clay Masonry (2020) <https://www.thinkbrick.com.au/Technical/Manuals/DownloadManual/12?ManualName=Manual%2010-Construction%20guidelines.pdf>. Accessed 20 July 2020
36. Australian Standard (2014) Methods of testing concrete; Preparation of concrete mixes in the laboratory. AS 1012.2: 2014
37. Australian Standard (2014) Methods of testing concrete; method for making and curing concrete. AS 1012.8.1: 2014
38. AS 2350 (Australian Standard) (2016) Methods of testing Portland, blended and masonry cements. Sydney
39. Binda L, de Vekey B, Acharhabi A, Baronio G, Bekker P, Borchelt G, Groot C (1998) RILEM TC 127-MS: tests for masonry materials and structures. *Mater Struct* 31(205):2–19
40. Breyse D (2012) Nondestructive evaluation of concrete strength: an historical review and a new perspective by combining NDT methods. *Constr Build Mater* 33:139–163
41. Nakamura H, Nanri T, Miura T, Roy S (2018) Experimental investigation of compressive strength and compressive fracture energy of longitudinally cracked concrete. *Cement Concr Compos* 93:1–18
42. Pluijm RVD (1999) Out-of-plane bending of masonry, behavior and strength. Ph.D. Thesis, Eindhoven University of Technology, Eindhoven
43. Benedetti A, Pelà L and Aprile A (2008) Masonry properties determination via splitting tests on cores with a rotated mortar layer. In: *Proceedings of 8th international seminar on structural masonry*, Istanbul
44. Vu XH, Malecot Y, Daudeville L, Buzaud E (2009) Experimental analysis of concrete behavior under high confinement: effect of the saturation ratio. *Int J Solids Struct* 46(5):1105–1120

Publisher's Note Springer Nature remains neutral with regard to jurisdictional claims in published maps and institutional affiliations.

